



Aerosol iron speciation and seasonal variation of iron oxidation state over the western Antarctic Peninsula

Songyun Fan^a, Yuan Gao^{a,*}, Barry Lai^b, Evert J. Elzinga^a, Shun Yu^a

^a Department of Earth and Environmental Sciences, Rutgers University, Newark, NJ 07102, USA

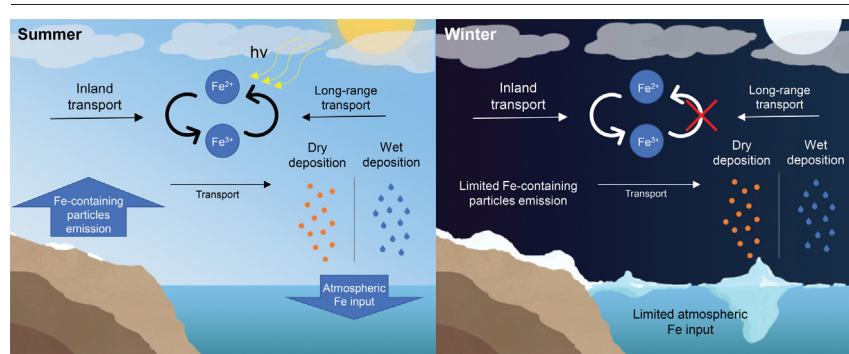
^b Advanced Photon Source, Argonne National Laboratory, Argonne, IL 60439, USA



HIGHLIGHTS

- Hematite and biotite are the most abundant Fe-containing minerals in aerosols in both summer and winter.
- The percentage of Fe(II) in total aerosol Fe was significantly higher in summer than in winter.
- The observed Fe-containing particles were likely associated with regional crustal emissions affected by snow/ice cover.

GRAPHICAL ABSTRACT



ARTICLE INFO

Article history:

Received 7 December 2021

Received in revised form 7 February 2022

Accepted 11 February 2022

Available online 16 February 2022

Editor: Hai Guo

Keywords:

Fe oxidation states
Antarctic Peninsula
Aerosols
XANES
Fe mineralogy

ABSTRACT

The iron (Fe) speciation and oxidation state have been considered critical factors affecting Fe solubility in the atmosphere and bioavailability in the surface ocean. In this study, elemental composition and Fe speciation in aerosol samples collected at the Palmer Station in the West Antarctic Peninsula were determined using synchrotron-based X-ray fluorescence (XRF) and X-ray Absorption Near-Edge Structure (XANES) spectroscopy. The elemental composition of coarse-mode (>1 μm) Fe-containing particles suggests that the region's crustal emission is the primary source of aerosol Fe. The Fe minerals in these aerosol particles were predominantly hematite and biotite, but minor fractions of pyrite and ilmenite were observed as well. The Fe oxidation state showed an evident seasonal variation. The Fe(II) content accounted for 71% of the total Fe in the austral summer, while this fraction dropped to 60% in the austral winter. Multivariate linear models involving meteorological parameters suggested that the wind speed, relative humidity, and solar irradiance were the factors that significantly controlled the percentage of Fe(II) in the austral summer. On the contrary, no relationship was found between these factors and the Fe(II) percentage in the austral winter, suggesting that atmospheric photoreduction and regional dust emission were limited. Moreover, the snow depth was significantly ($p < 0.05$) correlated with the aerosol Fe concentration, confirming the limiting effect of snow/ice cover on the regional dust emission. Given that the Antarctic Peninsula has experienced rapid warming during recent decades, the ice-free areas in the Antarctic Peninsula may act as potential dust sources.

1. Introduction

Iron (Fe) serves as an essential micronutrient for ocean primary production and regulates global biogeochemical cycles (Falkowski, 1997; Martin and Fitzwater, 1988; Sarmiento and Gruber, 2006; Tagliabue et al., 2017). The emission, transport, and deposition of atmospheric dust is an important pathway supplying Fe to the surface layers of the remote oceans

* Corresponding author.

E-mail address: yuangaoh@newark.rutgers.edu (Y. Gao).

(Duce and Tindale, 1991; Fung et al., 2000; Jickells et al., 2005). Due to insufficient dust supply, iron deficiency has been confirmed as a limiting factor in the vast high-nutrient low-chlorophyll (HNLC) regions in the Southern Ocean (Boyd et al., 2007; Coale et al., 2004). Previous modeling studies and satellite observations have demonstrated that aeolian dust over the Southern Ocean and Antarctica mainly originates from arid and unvegetated regions in Australia, South Africa, and South America (Gassó et al., 2010; Ito and Shi, 2016; Li et al., 2008; Mahowald, 2007). In recent years, the impacts of likely local dust sources were reported in Antarctica (Bory et al., 2010; Delmonte et al., 2013; Gao et al., 2013; Gao et al., 2020; Winton et al., 2014).

Fe-containing particles derived from different sources (e.g., desert dust, fuel combustion) may have vastly different mineralogical properties leading to considerable variability in Fe solubility and bioavailability (Journet et al., 2008; Schroth et al., 2009; Spolaor et al., 2013; Ito et al., 2019). For instance, Fe(III) minerals such as hematite, goethite, and ferrihydrite, dominate Fe mineralogy in desert dust particles, whereas a significant fraction of Fe in glacial flour is Fe(II) silicate; consequently, the Fe fractional solubility of dust particles can be one to two magnitudes lower than glacial flour (Schroth et al., 2009). Besides, anthropogenic combustion was suggested as a critical source, which contributes more than 40% of total soluble Fe to the Southern Ocean due to the presence of highly soluble coquimbite ($\text{Fe}_2(\text{SO}_4)_4 \cdot 9\text{H}_2\text{O}$) and nanosized Fe_3O_4 aggregates in oil fly ash (Ito, 2015). In addition to the Fe origination, aeolian Fe speciation is also controlled by atmospheric processes. Acidic and photochemical reactions have proven to influence the Fe solubility by modifying the Fe speciation and oxidation state in aerosols (Ingall et al., 2018; Longo et al., 2016; Zhu et al., 1992). Moreover, seasonal variation has also been found in the atmospheric Fe properties over the global ocean (Gao et al., 2001). Large seasonal differences between austral summer and winter in the meteorological parameters associated with atmospheric chemical reactions were observed in Antarctic Peninsula (Kim et al., 2017). For instance, the highest monthly mean air temperature in austral summer can be ~ 10 to 15 °C higher than the coldest month in austral winter. Such a difference in temperature may affect Fe speciation as ice crystals in the atmosphere may promote Fe photoreduction (Desboeufs et al., 2001). In addition, the highest monthly mean solar radiation is ~ 200 W m^{-2} in the austral summer, whereas this number drops to 0 during the austral winter. Therefore, Fe speciation and oxidation states in aerosols are likely to exhibit seasonal variability.

In past decades, the environment in the Antarctic Peninsula has experienced dramatic changes (Znój et al., 2017). Rapid regional warming (Bromwich et al., 2013; Vaughan et al., 2003) has caused glacier retreat (Cook et al., 2016), snow cover reduction (Fox and Cooper, 1998), and summer melting unprecedented over the past thousand years (Abram et al., 2013). Several ice-free areas have been reported on James Ross Island, King George Island, and Anvers Island, among others, in the Antarctic Peninsula (Bockheim et al., 2013). The low precipitation rate and high wind speed conditions in this region likely make ice-free areas active dust sources, contributing Fe-containing particles to the air (Kavan et al., 2018). High-resolution records of ice core from James Ross Island showed that the dust concentrations and deposition fluxes more than doubled during the 20th century under ~ 1 °C warming (McConnell et al., 2007). Besides changes in dust fluxes, measuring aerosol Fe speciation is needed as well to better assess the impacts of environmental changes on the supply of Fe to the oceans in this region. Nonetheless, most aerosol studies in this region focused on measuring or estimating the total concentrations and deposition fluxes of Fe (Artaxo et al., 1992; Correia et al., 1998; Gao et al., 2020; Préndez et al., 2009). Field measurements of aerosol Fe speciation and its variation in this region are still inadequate.

Aerosol Fe speciation and oxidation states can be characterized using various methods. A commonly used method involves aqueous extraction of Fe from aerosol samples followed by spectrophotometric analysis of the extractant solutes (Gao et al., 2013; Gao et al., 2019; Longo et al., 2016; Xu and Gao, 2017). This method provides limited information on the solid-phase Fe speciation in aerosols. Mössbauer spectroscopy has also been used to measure the Fe speciation and oxidation state in aerosol

samples (Fu et al., 2012). However, this technique requires significant sample mass (~ 1 g aerosol sample) (Hoffmann et al., 1996), making it difficult to apply to the determination of Fe in Antarctica aerosol samples due to the low concentrations of aerosol Fe in this region (Gao et al., 2020). In recent years, synchrotron-based X-ray Absorption Near-Edge Structure (XANES) spectroscopy has been used to analyze the speciation and oxidation state of Fe in aerosol particles (Elzinga et al., 2011; Ingall et al., 2018; Kurisu et al., 2019; Longo et al., 2016; Oakes et al., 2012; Pattammattel et al., 2021; Takahashi et al., 2011). This technique requires only a small amount of aerosol material and no sample processing.

This study focuses on characterizing aerosol Fe mineralogy and oxidation states for a better understanding of the sources and bioavailability of aerosol Fe in the Antarctic Peninsula. Our previous study determined the concentrations of total Fe and soluble Fe species in aerosols in this region (Gao et al., 2020) and suggested that local and regional dust emissions might affect the aerosol Fe speciation. To further explore this issue, combined microscopic X-ray fluorescence (XRF) and Fe K-edge XANES spectroscopy were deployed to analyze the solid phase speciation of Fe in aerosol particles collected at the Palmer Station in the western Antarctic Peninsula. The results of this study are then combined with the total Fe concentrations to further discuss the factors that affect local dust emissions in this region.

2. Material and methods

2.1. Sample collection

Aerosol particles were sampled at Palmer Station ($64^{\circ}46'S$ $64^{\circ}03'W$) on the Anvers Island in the western Antarctic Peninsula (Fig. 1). Both size-segregated and bulk samples were collected. Detailed sampling information is given in Gao et al. (2020) and Fan et al. (2021). In brief, bulk aerosol samples were collected on pre-acid cleaned cellulose filters (Whatman 41, Maidstone, UK) by a high-volume sampler with ca. $1 \text{ m}^3 \text{ min}^{-1}$ flow rate between Nov 2015 and Jan 2017. Size-segregated aerosol samples were collected on Teflon filters ($1 \mu\text{m}$ pore size, 47 mm diameter, Pall Corp., NY, USA) by a ten-stage Micro-Orifice Uniform Deposit Impactor™ (MOUDI, MSP Corp., MN, USA) during two austral summers of 2015–2016 and 2016–2017. The sampling flow rate of the MOUDI sampler was 30 L min^{-1} . Based on the particle-size distributions of aerosol Fe measured by the MOUDI sampler, the highest mass concentrations of aerosol Fe were found on the 4th stages (50% cut-off size: $3.2 \mu\text{m}$) of MOUDI samples among all stages, and aerosol samples collected on that stage were selected for analysis in this study. Meteorological data, including solar irradiance and snow depth, were measured at the same site at Palmer Station.

2.2. Synchrotron-based X-ray spectroscopy analysis

The composition and Fe oxidation state of iron-bearing aerosol particles were analyzed using the facility on the 2-ID-D beamline at the Advanced Photon Source, located at Argonne National Laboratory, Lemont, Illinois. X-ray fluorescence (XRF) microscopy and X-ray absorption near-edge structure (XANES) spectroscopy were used to obtain elemental maps and Fe K-edge XANES scans, respectively. An energy dispersive Si-drift detector (Vortex EM, with a 50 mm^2 sensitive area and a $12.5 \mu\text{m}$ Be window; SII Nano-Technology, Northridge, CA) was used to collect the fluorescence signals. Samples were placed into a helium-filled chamber during scanning to minimize the absorbance of fluorescence signal by air molecules. Both samples and standards were analyzed following the same procedure.

Micro-XRF maps were collected first to locate the iron-containing particles on the sample filters and to analyze particle elemental compositions. Scanning was performed with the X-ray beam focused onto a ca. 200 nm diameter spot size with the X-ray focusing optics (zone plate and order sorting aperture). A randomly selected 1 mm^2 square was mapped in fly scan mode to identify Fe-bearing particles. Next, step scan mode was utilized to zoom in on iron-containing particles, which were mapped at a step size of 0.3 to $0.5 \mu\text{m}$ and a 0.5 s dwell time per step.

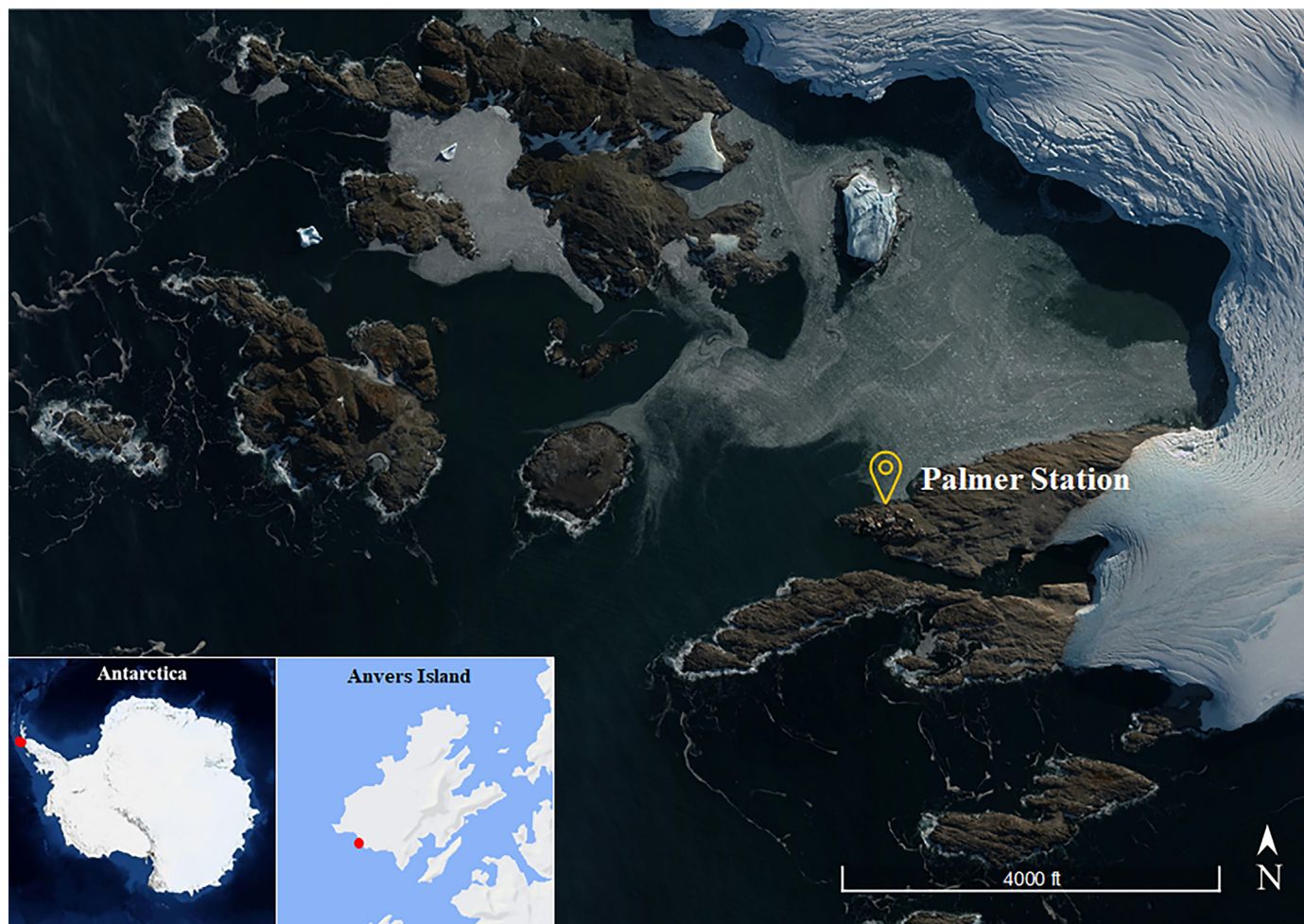


Fig. 1. Sampling site at Palmer Station on Anvers Island, western Antarctic Peninsula (satellite image credits: Google Earth Pro).

Selected iron-containing particles were also analyzed with micro Fe K-edge XANES measurements, which were collected in single particle mode using a focused X-ray beam with a $0.2 \mu\text{m}$ diameter. Because of time limitation, it was not possible to scan all particles on the sample filters. Therefore, XANES analyses of the aerosol samples were also performed in bulk mode, where the X-ray focusing optics were removed from the beam path allowing the unfocused X-ray beam to directly pass a ca. 0.4 mm^2 area on the filter. In both individual particle and bulk modes, the Fe XANES were scanned from 7100 to 7180 eV with a resolution of 0.5 eV and 0.5–5 s dwell time.

2.3. Data analysis

The elemental composition of iron-containing particles was obtained through the elemental maps generated by the micro-XRF data using MAPS software (Vogt, 2003). The X-ray for iron detection can also excite the elements with masses ranging from magnesium to manganese (Mg, Al, Si, P, S, Cl, K, Ca, Ti, V, Cr, Mn) and emit fluorescence signals. Then, the fluorescence datasets were converted to the area concentrations ($\mu\text{g cm}^{-2}$) and calibrated with National Bureau of Standards (NBS) reference material 1832 (Nietzold et al., 2018). To ensure the data quality, the XRF data was compared with the trace element concentrations measured by a total digestion method in Gao et al., 2020 and Fan et al., 2021 (Table S4). Principal component analysis (PCA) was used to determine the dominant sources of Fe-containing particles based on the elemental composition of these particles. The area concentrations from elemental maps were normalized by subtracting the mean and dividing the standard deviation before PCA. The PCA analysis was conducted using the “FactoMineR” (ver. 1.34) package in R (ver. 4.0.5) (Lê et al., 2008).

For determining the mineral composition of iron-containing particles, linear combination (LC) fitting was performed using the Athena software package (Ravel and Newville, 2005). A total of 12 Fe K-edge reference spectra were collected at the same beamline where the aerosol spectra were measured, including those for Fe(II) oxide (FeO , >99.6%, Sigma-Aldrich), Fe(II) oxalate ($\text{FeC}_2\text{O}_4 \cdot 2\text{H}_2\text{O}$, >99%, Thermo Fisher), Fe(II) sulfate ($\text{FeSO}_4 \cdot \text{xH}_2\text{O}$, >99.999%, Sigma-Aldrich), Fe(III) oxalate ($\text{Fe}_2(\text{C}_2\text{O}_4)_3 \cdot 6\text{H}_2\text{O}$, >97%, Thermo Fisher), Fe(III) sulfate ($\text{Fe}_2(\text{SO}_4)_3 \cdot \text{xH}_2\text{O}$, >97%, Sigma-Aldrich), Fe(III) phosphate ($\text{FePO}_4 \cdot 2\text{H}_2\text{O}$, Sigma-Aldrich), goethite ($\alpha\text{-Fe}(\text{OH})\text{O}$, Sigma-Aldrich), and hematite ($\alpha\text{-Fe}_2\text{O}_3$, 99.9%, Atlantic Equipment Engineers). All standards were measured in fluorescence mode using an unfocused X-ray beam. The spectra of biotite ($\text{K}(\text{Mg},\text{Fe})_3(\text{AlSi}_3\text{O}_{10})(\text{F},\text{OH})_2$), ferrihydrite ($\text{Fe}_2\text{O}_3 \cdot 0.5\text{H}_2\text{O}$), pyrite (FeS_2), and ilmenite (FeTiO_3) reported in Ingall et al. (2013), which were measured at the same beamline as well, were also included in the LC fitting analysis. The sample Fe-XANES spectra were fitted by up to 4 standards. The results of LC fitting were reflected by R-factor and reduced χ^2 . Standards with low contributions to the LC fitting (less than 5%) or which resulted in a poor fit were not included.

All the original Fe XANES spectra were background-corrected and normalized using Athena's built-in function. Due to the low iron signal in several samples, the measurements of Fe XANES were made 1–3 times. The replicated measurements of Fe XANES spectra were merged to generate one representative spectrum for each aerosol sample. Then, the pre-edge signals were subtracted baseline using XANES dactyloscope software (Klementiev, 2002) and fitted using PeakFit 4.0 by up to 5 Gaussian peaks to estimate the pre-edge centroid position. The percentage of Fe(II) (%Fe(II)) was roughly estimated through a linear equation (Eq.1) generated

by the mean pre-edge centroids of selected Fe-containing minerals. In this study, the mean pre-edge centroid of biotite and Fe(II) sulfate were selected to represent 0% Fe(III), whereas hematite and Fe(III) sulfate were selected to represent 100% Fe(III). Similar methods were applied in previous studies to convert the pre-edge centroid of Fe K-edge XANES to the % Fe oxidation state (Bajt et al., 1994; Oakes et al., 2012; Wilke et al., 2001).

$$\%Fe(II) = 100 - \frac{\text{Pre-edge Centroid Position} - 7113.11}{0.0129} \quad (1)$$

Multivariate linear models were used to discuss the impacts of meteorological conditions on the Fe oxidation state during the austral summer and winter. The best model was selected using stepwise regression and Bayesian information criterion (BIC) as the criterion.

3. Results and discussion

3.1. The source of Fe-containing particles

A total of 15 coarse-mode Fe-containing particles from 7 samples were scanned by the microscopic X-ray fluorescence. All particles were mixed with sea salt crystals (cubic shape, Chlorine) (Fig. 2). The elemental maps show that Fe in these particles was highly co-located with both Si and Al and partially co-located with Ti and Mn, whereas no significant correlation was found with other elements (Mg, P, S, Cl, K, Ca, V, Cr). The concentrations of Fe were significantly correlated with crustal elements Si and Al ($p < 0.01$). A relatively weak correlation was found between Fe and Ti/Mn (Ti: $r = 0.52$, $p = 0.047$; Mn: $r = 0.49$, $p = 0.066$), which might be caused by insufficient data points. In the Antarctic Peninsula, crustal emissions are an important contributor to aerosol Al, Si, and Ti (Artaxo et al., 1992). The

significant correlations between Fe and these crustal elements are clear evidence that the crustal emission greatly controls the coarse-mode Fe-containing particles in aerosols at Palmer Station as observed in Gao et al. (2020).

Principal component analysis (PCA) was performed to further investigate the major sources of Fe-containing particles (Fig. S1). The first principal component explains 65.9% of the variance and has a high positive association with most elements (Mg, S, Cl, K, Ca, Ti, V, Cr, Mn). The second principal component explains 20.5% of the variance, with high loading of Al, Si, and Fe. The third component showed high loading for P only and explained 7.4% of the variance. These three components explain more than 90% of the variance, and all have an eigenvalue greater than or close to 1. The results of PCA suggest the aerosol elemental composition was primarily affected by three main sources.

In the Southern Ocean and coastal Antarctica, aerosol trace elements are derived from various sources, including sea-salt emission, crustal sources, anthropogenic emissions, etc. (Weller et al., 2008; Xu and Gao, 2014). Given that Palmer Station is a coastal site in the Antarctic Peninsula, sea-salt aerosol was reported as the dominant species, contributing to a considerable amount of Mg, S, Cl, K, Ca in the air. In addition, remote and regional crustal emissions are the main sources of some elements, including Al, Si, P, Ti, V, and Mn, in the Antarctic Peninsula (Artaxo et al., 1992; Fan et al., 2021). During the sampling periods, the particle size distributions of crustal elements (Al, Ti, Mn, Fe) in aerosols were mostly accumulated in coarse mode particles ($>1.8 \mu\text{m}$), suggesting that these crustal elements in aerosols were likely dominated by regional sources (Gao et al., 2020; Fan et al., 2021). The results of Fe mineralogy also show that local crustal sources played a more important role than remote sources and are discussed in Section 3.2. At Palmer Station, a modest enrichment in P was observed, suggesting that the resuspension of regional soil particles might deliver P-

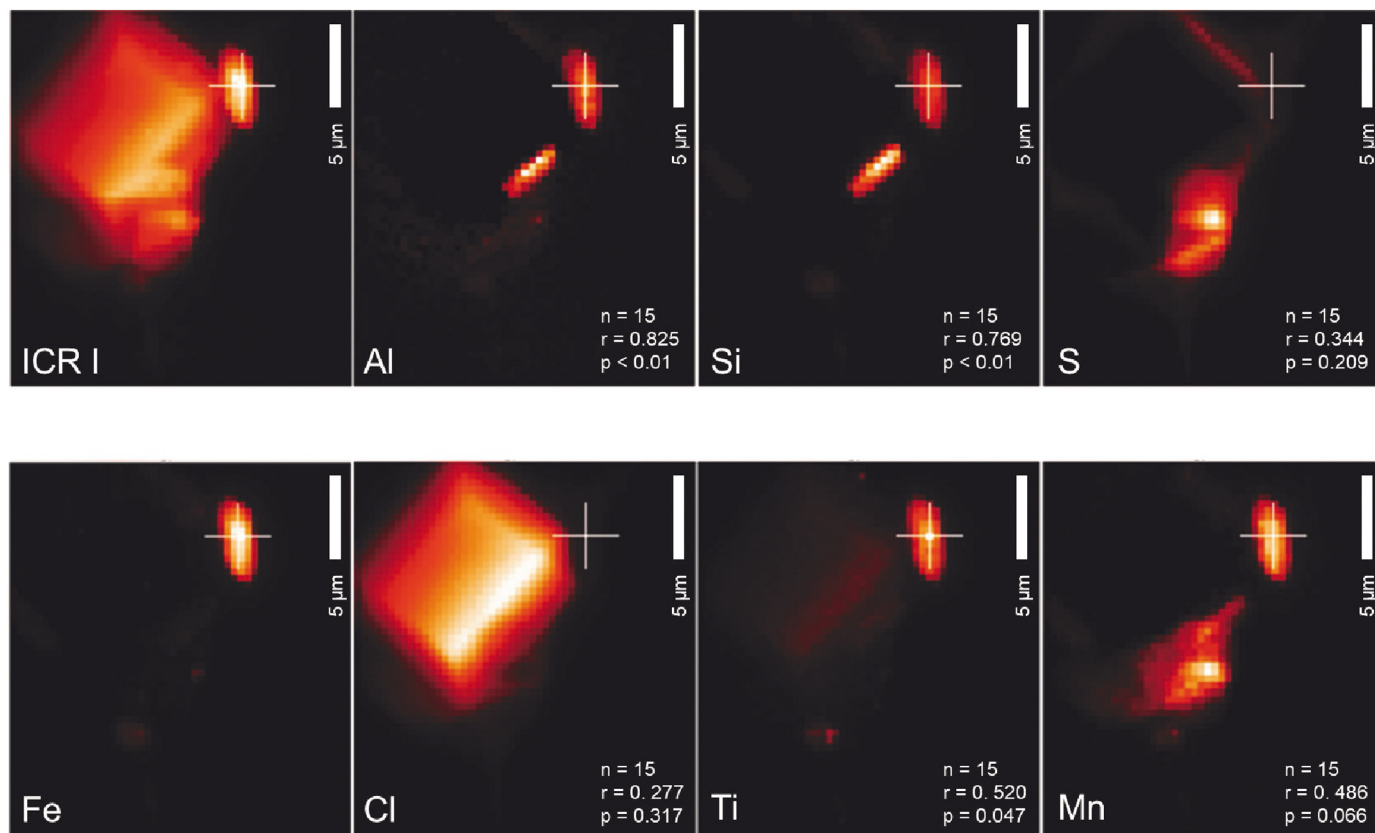


Fig. 2. Elemental maps ($20 \times 22 \mu\text{m}$) of aluminum (Al), silicon (Si), sulfur (S), chlorine (Cl), titanium (Ti), manganese (Mn), and iron (Fe) of an iron-containing particle on the PM9A-4 Teflon sample filter. Input Count Rate (ICR) was used here to show the overall shape of the individual particle. The center of the iron-containing region is marked by the white cross on the same position in each map. Information about the correlation between Fe and each element, including sample number (n), Pearson correlation coefficient (r), and p-value (p), is shown in the lower right corner of each map.

enriched particles to the air from bird colonies (Otero et al., 2018). Moreover, Polluted aerosols containing Cr derived from long-range transport were also detected in this region (Artaxo et al., 1992). The concentrations and particle size distributions of Pb in aerosols observed at Palmer Station were occasionally affected by air masses from the South America, suggesting the anthropogenic impact through long-range transport (Fan et al., 2021). Therefore, we conclude that three components derived from the PCA results represent major contributions from (1) the mixture of sea salt aerosol, remote crustal emission, and other remote sources, (2) local crustal emission, and (3) P-enriched aerosols that might derive from specific local biogenic emission, respectively.

3.2. Iron mineralogy in Fe-containing particles

The Fe mineralogy was determined by LC fitting of the bulk Fe K-edge XANES spectra collected for the aerosols (Fig. 3). Hematite and biotite were the most abundant Fe-minerals, dominating the Fe mineralogy of the bulk aerosols in both austral summer and winter. The LC fits of the coarse-mode size-segregated samples yielded similar results but with a higher percentage of hematite (Fig. 3). The fraction of biotite slightly decreased during the winter season. In Antarctic Peninsula, both hematite and biotite were previously found in soils, sediments, and rocks (Armstrong and Willan, 1996; Hawkes and Littlefair, 1981). Satellite-based remote sensing data further confirmed that biotite is widely distributed in the Antarctic Peninsula (Pour et al., 2018). In addition, a relatively small fraction of pyrite and ilmenite was observed in the bulk samples as well (Fig. 3). Sand-sized pyrite originating from quartz-pyrite rocks is distributed widely in the Antarctic Peninsula (Cox et al., 1980; Khim and Yoon, 2003). Ilmenite is a titanium-iron oxide mineral. Minor amounts of ilmenite have been reported in aerosol samples collected from the Southern Ocean and coastal East Antarctica (Ingall et al., 2018). The ilmenite observed in summer samples may explain the weak correlation between Fe and Ti.

Hematite is the most common Fe mineral on Earth and accumulates as a secondary mineral in soils during weathering, particularly in tropical areas (Cornell and Schwertmann, 2003). A high abundance of hematite was found in African dust (Kandler et al., 2009). Thermodynamically, hematite is the most stable ferric oxide and has the lowest solubility (Jang et al., 2007). As Fe solubility is usually considered a critical index of Fe bioavailability (Sholkovitz et al., 2012), Fe present in hematite is considered to have a low bioavailability. Biotite, on the other hand, is a type of Fe(II)-phyllosilicate. Due to its high Fe(II) content, this mineral is relatively unstable, making biotite Fe more labile and bioavailable than the Fe(III) present in desert dust (Schroth et al., 2009; von der Heyden et al., 2012). The input of glaciogenic sediments enriched in Fe(II) silicates to the ocean has been suggested to mitigate Fe limitation at a low total Fe condition (Crusius et al., 2011; Shoenfelt et al., 2017), and the high proportion of Fe(II) silicates such as biotite and hornblende in natural dust could increase the bioavailable Fe flux by a factor of 15 to 20 during glacial periods (Shoenfelt et al., 2018). In Antarctica, mechanical weathering produces extensive rock flour composed of fine-size particles (below 1 μm to several μm) (Campbell and Claridge, 1987), which contain abundant biotite and are readily released into the air, thus acting as dust source material. Pyrite is another mineral with high Fe bioavailability, as it is readily weathered into bioavailable nanoparticles in seawater and utilized by marine microorganisms, and the low level of pyrite Southern Ocean marine sediments may be attributed to its high weatherability in these systems (Raiswell and Canfield, 1998).

The LC fits that included the Fe sulfate and Fe oxalate references yielded poor results (high R-factor), which indicates that these components were missing or only contributed limited fraction of Fe (<5%) in our samples. Fe(II) sulfate was widely found in marine aerosols as a product of acidic reactions and photoreduction in the atmosphere (Ingall et al., 2018). Fe-sulfates were also reported to be the primary components in the aerosol source materials from industrial combustion (Schroth et al., 2009). Their absence in aerosols observed at Palmer Station during this study suggests that Fe mineralogy is dominated by regional local dust emissions, and

that atmospheric processing does not modify the Fe mineralogy to a great extent. In addition, previous studies found organic complexed Fe increases the Fe solubility (Paris et al., 2011; Xu and Gao, 2008). Coastal areas in Antarctic Peninsula were suggested to contribute limited oxalate to the atmosphere compared with the nearby open ocean (Rinaldi et al., 2020), which might explain the lack of Fe-oxalate complex in aerosols in this region observed in this study.

Overall, our findings indicate that the aerosol Fe speciation at the Palmer Station is dominated by local dust emissions and that atmospheric acidic reactions appear to play a minor role in controlling the Fe mineralogy. The high fraction of Fe(II) minerals implies that Fe in dust derived from the Antarctic Peninsula has a high bioavailability following its deposition in adjacent seas.

3.3. Seasonal variation of aerosol Fe oxidation state

The results derived from fitting the pre-edge centroids of Fe XANES showed that the oxidation state of aerosol Fe in bulk aerosol samples varied considerably with seasons. The results of LC fitting suggested that the %Fe(II) accounted for 71% of the total aerosol Fe during the austral summer, whereas this fraction dropped to 60% during the austral winter. This suggests that aerosol Fe in Antarctic Peninsula is more bioavailable during the austral summer. The variation of Fe oxidation state can also be seen in the pre-edge centroids of the Fe XANES spectra (Fig. 4). Since the pre-edge centroid method of Wilke et al. (2001) was developed to determine the oxidation state of Fe oxide minerals, the presence of substantial of pyrite (a Fe(II)-sulfide) may affect the accuracy of the results. Therefore, this method was only applied to summer samples and suggested that the %Fe(II) ranged from 55% to 87% with a mean of 73%, which is consistent with the LC fit results.

To determine the factors that affect the aerosol Fe oxidation state, multivariate linear models were developed for the austral summer (Table 1). The model shows that relative humidity ($p < 0.01$), solar irradiance ($p < 0.01$), and wind speed ($p < 0.05$) all significantly affected the %Fe(II), explaining ~70% of the variation in the austral summer (adjusted R squared 0.682). The positive coefficients of relative humidity and solar irradiance suggest that the photochemical reduction of aerosol Fe is enhanced by high relative humidity and strong solar irradiance. A previous study has shown that photoreduction can effectively lower the Fe oxidation state in marine aerosols (Zhu et al., 1993), and the icy conditions in the polar region were suggested to make speed up this process (Kim et al., 2010). Atmospheric photoreduction converts less labile Fe to labile Fe in aqueous phase (Faust and Hoigné, 1990), and it is unlikely that the dominant Fe(II) species observed in this study (biotite, pyrite, and ilmenite) are the end products of photoreduction. Since the samples were collected at a coastal site, Fe(II) salts such as sulfates or phosphates are plausible products of atmospheric photoreduction. In addition, Fe-organic complexes found in dust aerosols can promote the photoreduction of Fe and increase the Fe fractional solubility (Pehkonen et al., 1993; Siefert et al., 1994). Some studies showed the Fe oxides nanoparticles attached on the surface of clay minerals or refractory Fe could be labile (Lieke et al., 2011; Scheuven et al., 2011) and participate photoreduction. Therefore, potential product Fe(II) may also exist as Fe(II)-organic complexes and/or as Fe(II) surface complexes on clay minerals or Fe(III)-(hydr)oxides. Gao et al. (2020) observed that that approximately 90% of the labile Fe was in the form of Fe(II) in our samples, but labile Fe accounted only for a small fraction in the total aerosol Fe, ranging from 2.5% to 7.3% with an average of 3.8% (Gao et al., 2020). As Fe species with low contribution were not included in LC fitting, the Fe(II) end products of photoreduction are likely not represented in the fit results because of low abundance.

The enhanced emission of Fe(II)-enriched source materials by high winds was another factor affecting the overall Fe oxidation state. The positive coefficient of wind speed in the summer model (Table 1) indicates that high wind conditions could significantly increase %Fe(II) in aerosols. The crustal enrichment factors of aerosol Fe in the samples collected at Palmer Station were close to 1, and most of aerosol Fe was accumulated in

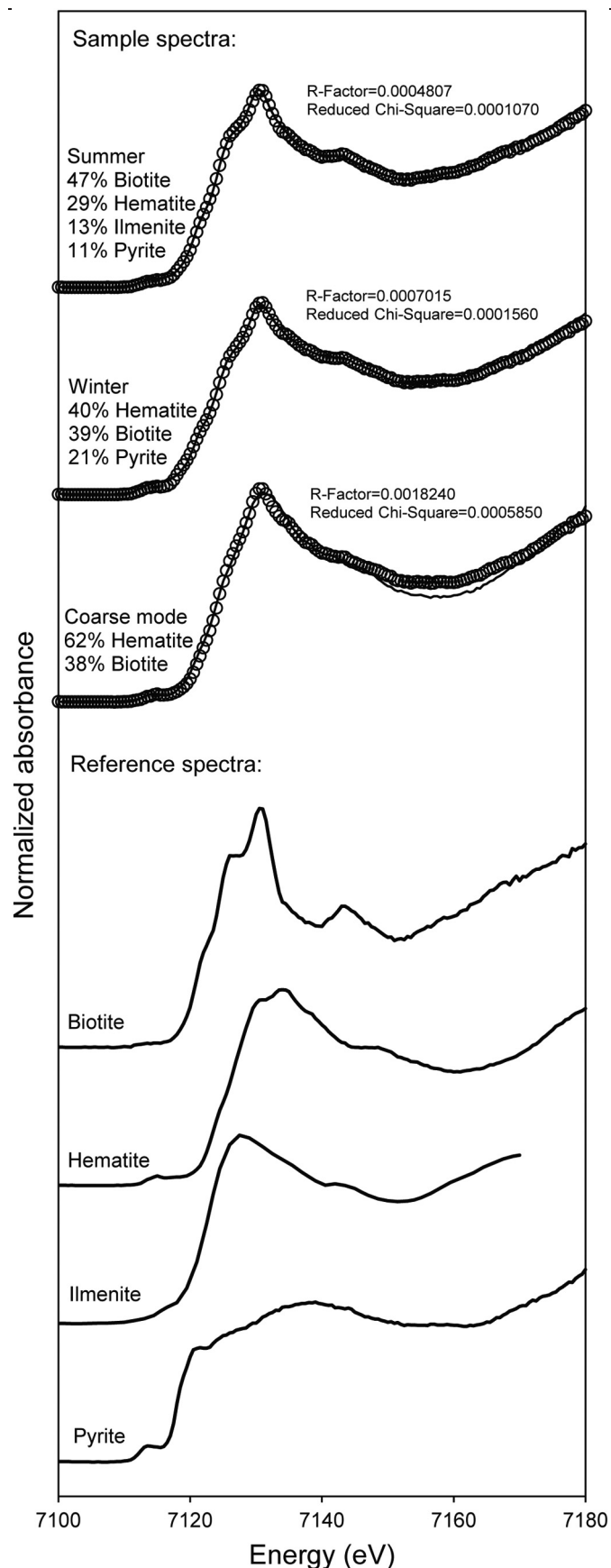


Fig. 3. Fits of Fe XANES spectra were conducted by linear combination (LC) fitting. The spectra of reference materials were collected at the same beamline. The solid line and cycle represent the measured spectra and fitting results, respectively.

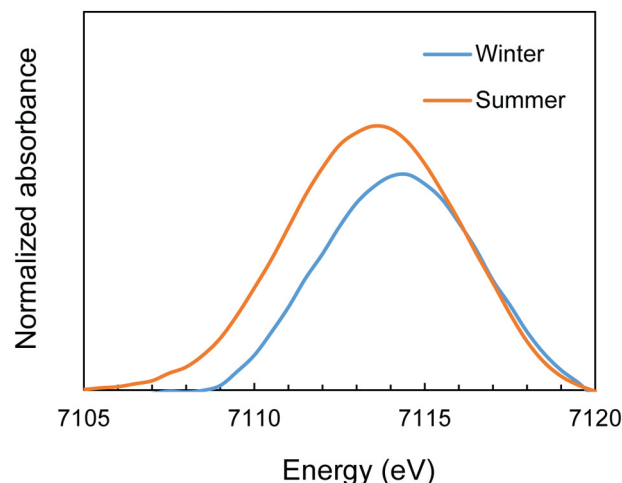


Fig. 4. A comparison of Fe XANES pre-edge centroids of summer and winter samples.

coarse-mode particles ($>1.8 \mu\text{m}$) (Gao et al., 2020). Those results suggested regional and local dust emissions are the dominant sources of aerosol Fe. High wind speeds could raise the amount of Fe-enriched dust emitted to the atmosphere. Similar Fe (II)-enriched glacial flours dominated by biotite minerals were reported in Alaska, accounting for ~ 70 to 80% of the total Fe (Schroth et al., 2009). Therefore, the relatively lower %Fe(II) in the winter might not be only caused by the cessation of photoreduction due to the lack of solar irradiance, but also partially attributed to the limited Fe(II)-enriched dust emissions in regional/local dust source areas.

3.4. The emission of Fe-containing particles

In Antarctica, higher dust deposition fluxes were reported in coastal regions, including the Antarctic Peninsula, and the dust particles in both aerosol (Gao et al., 2020) and ice-core samples (Albani et al., 2012; Bory et al., 2010; McConnell et al., 2007) were dominated by coarse-mode particles. The analyses of elemental composition and mineralogy reported in this study further suggest that the aerosol Fe-containing particles were primarily derived from crustal sources.

The warming of the Antarctic Peninsula has induced unprecedented summer melting in recent years (Abram et al., 2013). In 2009–2017, the West and Northeast Peninsula ice sheet deduced $42 \pm 5 \text{ Gt yr}^{-1}$ (Rignot et al., 2019), and there are up to 130 days per year with an air temperature above 0°C in the northern Antarctic Peninsula, causing an expansion of ice-free areas (Siegert et al., 2019). Increased exposure of ice-free land surfaces is likely to lead to considerable changes in the dust fluxes in this region.

The satellite image reveals several ice-free areas on the Antarctic Peninsula including some areas around the Palmer Station (Fig. 1). The exposed rocks and soil might act as potential dust sources. To evaluate the impacts of snow/ice melting on the emission of dust, the snow depths were recorded during the summer sampling periods, and we assume this measurement reflects the variation of snow/ice-covered areas around the sampling site (Fig. 5). Higher average air temperature ($0.37 \pm 1.20^\circ\text{C}$) and thinner snow depth ($15.7 \pm 24.1 \text{ cm}$) were observed in the 2016–2017 summer

Table 1

Results from multivariate linear regression model of %Fe(II) in the total aerosol Fe during the summer.

	Coefficients	Stand error	p-value
Intercept	-109	37.4	0.02
Wind speed	2.88	1.18	0.04
Relative humidity	1.66	0.330	0.001
Solar irradiance	0.224	0.0582	0.005
Multiple R ²	0.769	Adjusted R ²	0.682
F-statistics	p-value = 0.006		

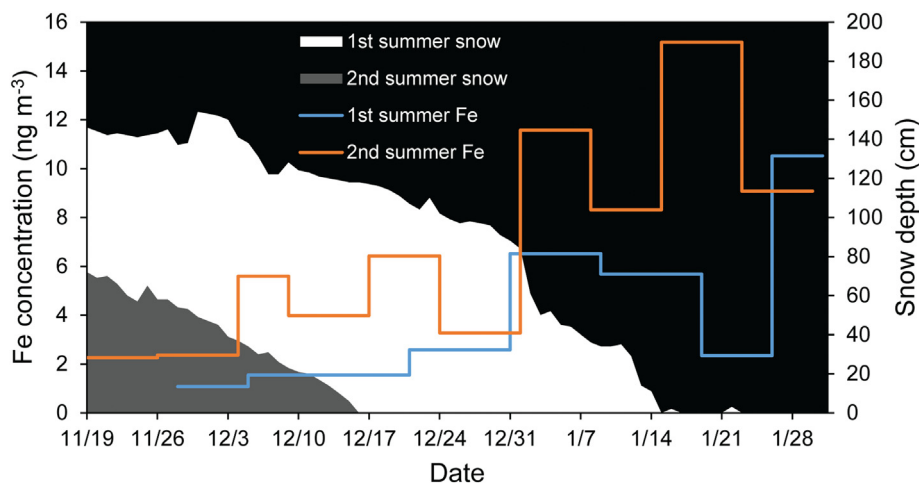


Fig. 5. The variation of atmospheric Fe concentrations (solid lines) during 2015–2016 (blue) and 2016–2017 (orange) austral summer. The snow depth in 2015–2016 (shaded white) and 2016–2017 (shaded grey) austral summer were measured in the “backyard” of Palmer Station. The snow depth data before December 1, 2015, and after January 28, 2016, were missing.

than those in the 2015–2016 summer (mean air temperature: 1.53 ± 1.27 °C; mean snow depth: 69.2 ± 59.6 cm). Significant linear relationships ($p < 0.05$) were found between snow depth and aerosol Fe concentrations (Fig. 6). In addition, it has been suggested that a slight increase in temperature might cause rapid melting and significant expansion in ice-free areas (Abram et al., 2013). Therefore, the impact of warming on regional dust emission could severely affect the crustal Fe emission. Moreover, the current melting is expected to accelerate due to the increased upwelling of warmer circumpolar deep water (Siebert et al., 2019). By the end of this century, the total ice-free area in Antarctica could expand 25%, and more than 85% of the new ice-free area will emerge in the Antarctic Peninsula (Lee et al., 2017). With ice-free area expanding, some areas in the Antarctic Peninsula has potential to be a forthcoming dust source and contributes a noticeable fraction of Fe(II) into the atmosphere.

4. Conclusions and implications

This study suggests that the regional dust emission in ice-free areas of the Antarctic Peninsula dominates the local aerosol Fe speciation. A large portion of Fe is in the form of Fe(II) minerals, mostly biotite, in both coarse-mode and bulk samples. Similar results were reported in Alaska glacial flours with

higher Fe solubility and bioavailability than for dust derived from mid-latitude deserts (Schroth et al., 2009). In addition, the aerosol Fe oxidation state exhibited an evident seasonal variation. High %Fe(II) was observed in the austral summer, attributed to the atmospheric photoreduction and stronger regional Fe(II)-enriched dust emissions. On the other hand, the atmospheric photoreduction was suspended due to the lack of solar radiation in the austral winter. The Fe(II)-enriched dust emission was greatly restricted during the winter because of the snow/ice cover. Nowadays, Antarctic Peninsula is experiencing rapid warming. The expansion of ice-free areas is likely to release more Fe(II)-enriched dust into the air. Although the atmospheric dust deposition only contributes a small amount of Fe to the adjacent seas (Gao et al., 2020), the importance of regional dust emissions in the Antarctic Peninsula may need to be re-evaluated.

CRediT authorship contribution statement

Songyun Fan: Lab experiments, Data analysis, Writing-Original draft preparation. **Yuan Gao:** Conceptualization, Project administration, Lab experiments, Writing-Reviewing and Editing, Funding acquisition. **Barry Lai:** Lab experiments, Writing-Reviewing and Editing, Data analysis. **Evert J. Elzinga:** Writing-Reviewing and Editing. **Shun Yu:** Resources, Sampling.

Declaration of competing interest

The authors declare that they have no known competing financial interests or personal relationships that could have appeared to influence the work reported in this paper.

Acknowledgements

This research was sponsored by the US National Science Foundation Grant OPP-1341494 and OCE-2048858 to YG. Sample analyses were performed on Beamline 2-ID-D at the Advanced Photon Source, a US Department of Energy Office of Science User Facility operated by Argonne National Laboratory, under Contract No. DE-AC02-06CH11357. We are grateful to Pami Mukherjee, Rafael Jusino-Atresino, and Guojie Xu for assistance with air sampling preparation. This work would not have become possible without the support from the staff of Palmer Station and the US Antarctic Program.

Appendix A. Supplementary data

Supplementary data to this article can be found online at <https://doi.org/10.1016/j.scitotenv.2022.153890>.

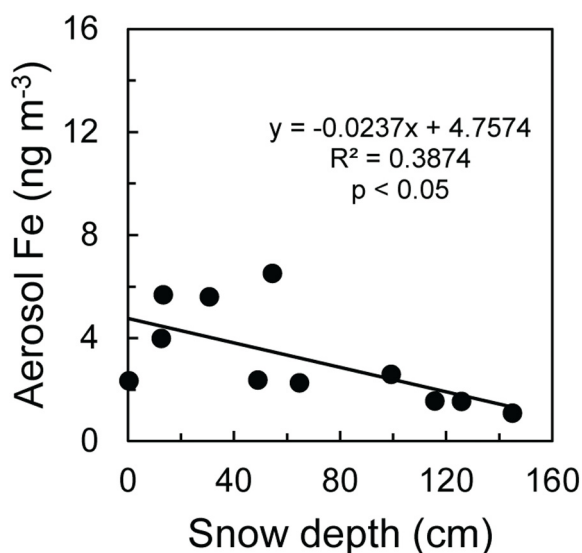


Fig. 6. Correlation between snow depth and aerosol Fe concentrations.

References

- Abram, N.J., Mulvaney, R., Wolff, E.W., Triest, J., Kipfstuhl, S., Trusel, L.D., Vimeux, F., Fleet, L., Arrowsmith, C., 2013. Acceleration of snow melt in an Antarctic peninsula ice core during the twentieth century. *Nat. Geosci.* 6 (5), 404–411. <https://doi.org/10.1038/ngeo1787>.
- Albani, S., Delmonte, B., Maggi, V., Baroni, C., Petit, J.R., Stenni, B., Mazzola, C., Frezzotti, M., 2012. Interpreting last glacial to holocene dust changes at talos dome (East Antarctica): implications for atmospheric variations from regional to hemispheric scales. *Clim. Past* 8 (2), 741–750. <https://doi.org/10.5194/cp-8-741-2012>.
- Armstrong, D., Willan, R., 1996. Orthomagmatic quartz and post-magmatic carbonate veins in a reported porphyry copper deposit, Andean Intrusive Suite, Livingston Island, South Shetland Islands. *Mineral. Deposita* 31 (4), 290–306.
- Artaxo, P., Rabello, M.L.C., Maenhaut, W., Grieken, R.V., 1992. Trace elements and individual particle analysis of atmospheric aerosols from the Antarctic peninsula. *Tellus B* 44 (4), 318–334. <https://doi.org/10.1034/j.1600-0889.1992.00010.x>.
- Bajt, S., Sutton, S.R., Delaney, J.S., 1994. X-ray microprobe analysis of iron oxidation states in silicates and oxides using X-ray absorption near edge structure (XANES). *Geochim. Cosmochim. Acta* 58 (23), 5209–5214. [https://doi.org/10.1016/0016-7037\(94\)90305-0](https://doi.org/10.1016/0016-7037(94)90305-0).
- Bockheim, J., Vieira, G., Ramos, M., López-Martínez, J., Serrano, E., Guglielmin, M., Wilhelm, K., Nieuwendam, A., 2013. Climate warming and permafrost dynamics in the Antarctic peninsula region. *Glob. Planet. Chang.* 100, 215–223. <https://doi.org/10.1016/j.gloplacha.2012.10.018>.
- Bory, A., Wolff, E., Mulvaney, R., Jagoutz, E., Wegner, A., Ruth, U., Elderfield, H., 2010. Multiple sources supply eolian mineral dust to the Atlantic sector of coastal Antarctica: evidence from recent snow layers at the top of Berkner Island ice sheet. *Earth Planet. Sci. Lett.* 291 (1), 138–148. <https://doi.org/10.1016/j.epsl.2010.01.006>.
- Boyd, P.W., Jickells, T., Law, C., Blain, S., Boyle, E., Buesseler, K., Coale, K., Cullen, J., De Baar, H.J., Follows, M., 2007. Mesoscale iron enrichment experiments 1993–2005: synthesis and future directions. *Science* 315 (5812), 612–617.
- Bromwich, D.H., Nicolas, J.P., Monaghan, A.J., Lazzara, M.A., Keller, L.M., Weidner, G.A., Wilson, A.B., 2013. Central West Antarctica among the most rapidly warming regions on earth. *Nat. Geosci.* 6 (2), 139–145. <https://doi.org/10.1038/ngeo1671>.
- Campbell, I.B., Claridge, G., 1987. *Antarctica: Soils, Weathering Processes and Environment*. Elsevier.
- Coale, K.H., et al., 2004. Southern Ocean iron enrichment experiment: carbon cycling in high- and low-Si waters. *Science* 304 (5669), 408–414. <https://doi.org/10.1126/science.1089778>.
- Cook, A.J., Holland, P.R., Meredith, M.P., Murray, T., Luckman, A., Vaughan, D.G., 2016. Ocean forcing of glacier retreat in the western Antarctic Peninsula. *Science* 353 (6296), 283–286. <https://doi.org/10.1126/science.aae0017>.
- Cornell, R.M., Schwertmann, U., 2003. *The Iron Oxides: Structure, Properties, Reactions, Occurrences and Uses*. John Wiley & Sons.
- Correia, A., Artaxo, P., Maenhaut, W., 1998. Monitoring of atmospheric aerosol particles on the Antarctic Peninsula. *Ann. Glaciol.* 27, 560–564. <https://doi.org/10.3189/1998AOG27-1-560-564>.
- Cox, C., Ciocanelea, R., Pride, D., 1980. Genesis of mineralization associated with andean intrusions, northern Antarctic peninsula region. *Antarct. J. US* 15 (5), 22–23.
- Crusius, J., Schroth, A.W., Gassó, S., Moy, C.M., Levy, R.C., Gatica, M., 2011. Glacial flour dust storms in the Gulf of Alaska: hydrologic and meteorological controls and their importance as a source of bioavailable iron. *Geophys. Res. Lett.* 38 (6). <https://doi.org/10.1029/2010GL046573>.
- Delmonte, B., Baroni, C., Andersson, P.S., Narcisi, B., Salvatore, M.C., Petit, J.R., Scarchilli, C., Frezzotti, M., Albani, S., Maggi, V., 2013. Modern and holocene aeolian dust variability from talos dome (Northern Victoria Land) to the interior of the Antarctic ice sheet. *Quat. Sci. Rev.* 64, 76–89. <https://doi.org/10.1016/j.quascirev.2012.11.033>.
- Desboeufs, K.V., Losno, R., Colin, J.L., 2001. Factors influencing aerosol solubility during cloud processes. *Atmos. Environ.* 35 (20), 3529–3537. [https://doi.org/10.1016/S1352-2310\(00\)00472-6](https://doi.org/10.1016/S1352-2310(00)00472-6).
- Duce, R.A., Tindale, N.W., 1991. Atmospheric transport of iron and its deposition in the ocean. *Limnol. Oceanogr.* 36 (8), 1715–1726.
- Elzinga, E.J., Gao, Y., Fitts, J.P., Tappero, R., 2011. Iron speciation in urban dust. *Atmos. Environ.* 45 (26), 4528–4532. <https://doi.org/10.1016/j.atmosenv.2011.05.042>.
- Falkowski, P.G., 1997. Evolution of the nitrogen cycle and its influence on the biological sequestration of CO₂ in the ocean. *Nature* 387 (6630), 272.
- Fan, S., Gao, Y., Sherrell, R.M., Yu, S., Bu, K., 2021. Concentrations, particle-size distributions, and dry deposition fluxes of aerosol trace elements over the Antarctic peninsula in austral summer. *Atmos. Chem. Phys.* 21 (3), 2105–2124. <https://doi.org/10.5194/acp-21-2105-2021>.
- Faust, B.C., Hoigné, J., 1990. Photolysis of Fe(III)-hydroxy complexes as sources of OH radicals in clouds, fog and rain. *Atmos. Environ. Part A* 24 (1), 79–89.
- Fox, A., Cooper, A., 1998. Climate-change indicators from archival aerial photography of the Antarctic peninsula. *Ann. Glaciol.* 27, 636–642.
- Fu, H., Lin, J., Shang, G., Dong, W., Grassian, V.H., Carmichael, G.R., Li, Y., Chen, J., 2012. Solubility of iron from combustion source particles in acidic media linked to iron speciation. *Environ. Sci. Technol.* 46 (20), 11119–11127. <https://doi.org/10.1021/es302558m>.
- Fung, I.Y., Meyn, S.K., Tegen, I., Doney, S.C., John, J.G., Bishop, J.K., 2000. Iron supply and demand in the upper ocean. *Glob. Biogeochem. Cycl.* 14 (1), 281–295.
- Gao, Y., Kaufman, Y.J., Tanré, D., Kolber, D., Falkowski, P.G., 2001. Seasonal distributions of aeolian iron fluxes to the global ocean. *Geophys. Res. Lett.* 28 (1), 29–32. <https://doi.org/10.1029/2000GL011926>.
- Gao, Y., Xu, G., Zhan, J., Zhang, J., Li, W., Lin, Q., Chen, L., Lin, H., 2013. Spatial and particle size distributions of atmospheric dissolvable iron in aerosols and its input to the Southern Ocean and coastal East Antarctica. *J. Geophys. Res. Atmos.* 118 (22), 12,634–12,648. <https://doi.org/10.1002/2013JD020367>.
- Gao, Y., Marsay, C.M., Yu, S., Fan, S., Mukherjee, P., Buck, C.S., Landing, W.M., 2019. Particle-size variability of aerosol iron and impact on iron solubility and dry deposition fluxes to the Arctic Ocean. *Sci. Rep.* 9, 16653. <https://doi.org/10.1038/s41598-019-52468-z>.
- Gao, Y., Yu, S., Sherrell, R.M., Fan, S., Bu, K., Anderson, J.R., 2020. Particle-size distributions and solubility of aerosol iron over the Antarctic peninsula during austral summer. *J. Geophys. Res. Atmos.* 125 (11), e2019JD032082. <https://doi.org/10.1029/2019JD032082>.
- Gassó, S., Stein, A., Marino, F., Castellano, E., Udisti, R., Ceratto, J., 2010. A combined observational and modeling approach to study modern dust transport from the Patagonia desert to East Antarctica. *Atmos. Chem. Phys.* 10 (17), 8287–8303. <https://doi.org/10.5194/acp-10-8287-2010>.
- Hawkes, D.D., Littlefair, M.J., 1981. An occurrence of molybdenum, copper, and iron mineralization in the Argentine Islands, West Antarctica. *Economic Geology* 76 (4), 898–904. <https://doi.org/10.2113/gsecongeo.76.4.898>.
- von der Heyden, B.P., Roychoudhury, A.N., Mtshali, T.N., Tyliczcak, T., Myneni, S.C.B., 2012. Chemically and geographically distinct solid-phase iron pools in the Southern Ocean. *Science* 338 (6111), 1199–1201. <https://doi.org/10.1126/science.1227504>.
- Hoffmann, P., Dedik, A.N., Ensling, J., Weinbruch, S., Weber, S., Sinner, T., Gütlich, P., Ortner, H.M., 1996. Speciation of iron in atmospheric aerosol samples. *J. Aerosol Sci.* 27 (2), 325–337. [https://doi.org/10.1016/0021-8502\(95\)00563-3](https://doi.org/10.1016/0021-8502(95)00563-3).
- Ingall, E.D., Diaz, J.M., Longo, A.F., Oakes, M., Finney, L., Vogt, S., Lai, B., Yager, P.L., Twining, B.S., Brandes, J.A., 2013. Role of biogenic silica in the removal of iron from the Antarctic seas. *Nat. Commun.* 4 (1), 1981. <https://doi.org/10.1038/ncomms2981>.
- Ingall, E.D., et al., 2018. Enhanced iron solubility at low pH in global aerosols. *Atmosphere* 9 (5), 201.
- Ito, A., 2015. Atmospheric processing of combustion aerosols as a source of bioavailable iron. *Environ. Sci. Technol. Lett.* 2 (3), 70–75. <https://doi.org/10.1021/acs.estlett.5b00007>.
- Ito, A., Shi, Z., 2016. Delivery of anthropogenic bioavailable iron from mineral dust and combustion aerosols to the ocean. *Atmos. Chem. Phys.* 16 (1), 85–99. <https://doi.org/10.5194/acp-16-85-2016>.
- Ito, A., et al., 2019. Pyrogenic iron: the missing link to high iron solubility in aerosols. *Science Advances* 5 (5), eaau7671. <https://doi.org/10.1126/sciadv.aau7671>.
- Jang, J.-H., Dempsey, B.A., Burgos, W.D., 2007. Solubility of hematite revisited: effects of hydration. *Environ. Sci. Technol.* 41 (21), 7303–7308. <https://doi.org/10.1021/es070535t>.
- Jickells, T.D., et al., 2005. Global iron connections between desert dust, ocean biogeochemistry, and climate. *Science* 308 (5718), 67–71. <https://doi.org/10.1126/science.1105959>.
- Journet, E., Desboeufs, K.V., Caquineau, S., Colin, J.L., 2008. Mineralogy as a critical factor of dust iron solubility. *Geophys. Res. Lett.* 35 (7).
- Kandler, K., et al., 2009. Size distribution, mass concentration, chemical and mineralogical composition and derived optical parameters of the boundary layer aerosol at tinfou, Morocco, during SAMUM 2006. *Tellus B* 61 (1), 32–50. <https://doi.org/10.1111/j.1600-0889.2008.00385.x>.
- Kavan, J., Dagsson-Waldhauserova, P., Renard, J.B., Láská, K., Ambrožová, K., 2018. Aerosol concentrations in relationship to local atmospheric conditions on James Ross island, Antarctica. *Frontiers Earth Sci.* 6 (207). <https://doi.org/10.3389/feart.2018.00207>.
- Khim, B.-K., Yoon, H.I., 2003. Postglacial marine environmental changes in Maxwell Bay, King George Island, West Antarctica. *Polar Res.* 22 (2), 341–353. <https://doi.org/10.1111/j.1751-8369.2003.tb00116.x>.
- Kim, K., Choi, W., Hoffmann, M.R., Yoon, H.-I., Park, B.-K., 2010. Photoreductive dissolution of iron oxides trapped in ice and its environmental implications. *Environ. Sci. Technol.* 44 (11), 4142–4148. <https://doi.org/10.1021/es9037808>.
- Kim, J., Yoon, Y.J., Gim, Y., Kang, H.J., Choi, J.H., Park, K.T., Lee, B.Y., 2017. Seasonal variations in physical characteristics of aerosol particles at the King Sejong Station, Antarctic Peninsula. *Atmos. Chem. Phys.* 17 (21), 12985–12999. <https://doi.org/10.5194/acp-17-12985-2017>.
- Klementiev, K., 2002. XANES Dactyloscope for Windows, KV Klementiev, XANES Dactyloscope for Windows. www.desy.de/~klmn/xanda.html.
- Kurusu, M., Adachi, K., Sakata, K., Takahashi, Y., 2019. Stable isotope ratios of combustion iron produced by evaporation in a steel plant. *ACS Earth Space Chem.* 3 (4), 588–598.
- Lê, S., Josse, J., Husson, F., 2008. FactoMineR: an R package for multivariate analysis. *J. Stat. Softw.* 25 (1), 1–18. <https://doi.org/10.18637/jss.v025.i01>.
- Lee, J.R., Raymond, B., Bracegirdle, T.J., Chadès, I., Fuller, R.A., Shaw, J.D., Terauds, A., 2017. Climate change drives expansion of Antarctic ice-free habitat. *Nature* 547 (7661), 49–54. <https://doi.org/10.1038/nature22996>.
- Li, F., Ginoux, P., Ramaswamy, V., 2008. Distribution, transport, and deposition of mineral dust in the Southern Ocean and Antarctica: contribution of major sources. *J. Geophys. Res.* 113 (D10). <https://doi.org/10.1029/2007jd009190>.
- Lieke, K., Kandler, K., Scheuvs, D., Emmel, C., Glahn, C.V., Petzold, A., Schütz, L., 2011. Particle chemical properties in the vertical column based on aircraft observations in the vicinity of Cape Verde Islands. *Tellus B* 63 (4), 497–511.
- Longo, A.F., Feng, Y., Lai, B., Landing, W.M., Shelley, R.U., Nenes, A., Mihalopoulos, N., Violaki, K., Ingall, E.D., 2016. Influence of atmospheric processes on the solubility and composition of iron in saharan dust. *Environ. Sci. Technol.* 50 (13), 6912–6920. <https://doi.org/10.1021/acs.est.6b02605>.
- Mahowald, N.M., 2007. Anthropocene changes in desert area: sensitivity to climate model predictions. *Geophys. Res. Lett.* 34 (18). <https://doi.org/10.1029/2007gl030472>.
- Martin, J.H., Fitzwater, S.E., 1988. Iron deficiency limits phytoplankton growth in the north-east Pacific subarctic. *Nature* 331 (6154), 341.
- McCannell, J.R., Aristarain, A.J., Banta, J.R., Edwards, P.R., Simões, J.C., 2007. 20th-century doubling in dust archived in an Antarctic peninsula ice core parallels climate change and desertification in South America. *Proc. Natl. Acad. Sci.* 104 (14), 5743–5748. <https://doi.org/10.1073/pnas.0607657104>.
- Nietzold, T., West, B.M., Stuckelberger, M., Lai, B., Vogt, S., Bertoni, M.I., 2018. Quantifying X-ray fluorescence data using MAPS. *J. Vis. Exp.* 132, 56042. <https://doi.org/10.3791/56042>.

- Oakes, M., Weber, R.J., Lai, B., Russell, A., Ingall, E.D., 2012. Characterization of iron speciation in urban and rural single particles using XANES spectroscopy and micro X-ray fluorescence measurements: investigating the relationship between speciation and fractional iron solubility. *Atmos. Chem. Phys.* 12 (2), 745–756. <https://doi.org/10.5194/acp-12-745-2012>.
- Otero, X.L., De La Peña-Lastra, S., Pérez-Alberti, A., Ferreira, T.O., Huerta-Díaz, M.A., 2018. Seabird colonies as important global drivers in the nitrogen and phosphorus cycles. *Nat. Commun.* 9 (1), 246. <https://doi.org/10.1038/s41467-017-02446-8>.
- Paris, R., Desboeufs, K.V., Journet, E., 2011. Variability of dust iron solubility in atmospheric waters: investigation of the role of oxalate organic complexation. *Atmos. Environ.* 45 (36), 6510–6517. <https://doi.org/10.1016/j.atmosenv.2011.08.068>.
- Pattammattel, A., Leppert, V.J., Aronstein, P., Robinson, M., Mousavi, A., Sioutas, C., Forman, H.J., O'Day, P.A., 2021. Iron speciation in particulate matter (PM_{2.5}) from urban Los Angeles using spectro-microscopy methods. *Atmos. Environ.* 245, 117988. <https://doi.org/10.1016/j.atmosenv.2020.117988>.
- Pehkonen, S.O., Siefert, R., Erel, Y., Webb, S., Hoffmann, M.R., 1993. Photoreduction of iron oxyhydroxides in the presence of important atmospheric organic compounds. *Environ. Sci. Technol.* 27 (10), 2056–2062.
- Pour, A.B., Hashim, M., Park, Y., Hong, J.K., 2018. Mapping alteration mineral zones and lithological units in Antarctic regions using spectral bands of ASTER remote sensing data. *Geocart. Int.* 33 (12), 1281–1306. <https://doi.org/10.1080/10106049.2017.1347207>.
- Préndez, M., Wachter, J., Vega, C., Flocchini, R.G., Wakayabashi, P., Morales, J.R., 2009. PM_{2.5} aerosols collected in the Antarctic peninsula with a solar powered sampler during austral summer periods. *Atmos. Environ.* 43 (34), 5575–5578. <https://doi.org/10.1016/j.atmosenv.2009.07.030>.
- Raiswell, R., Canfield, D.E., 1998. Sources of iron for pyrite formation in marine sediments. *Am. J. Sci.* 298 (3), 219–245. <https://doi.org/10.2475/ajs.298.3.219>.
- Ravel, B., Newville, M., 2005. ATHENA, ARTEMIS, HEPHAESTUS: data analysis for X-ray absorption spectroscopy using IFEFFIT. *J. Synchrotron Radiat.* 12 (4), 537–541.
- Rignot, E., Mouginot, J., Scheuchl, B., van den Broeke, M., van Wessem, M.J., Morlighem, M., 2019. Four decades of Antarctic ice sheet mass balance from 1979–2017. *Proc. Natl. Acad. Sci.* 116 (4), 1095–1103. <https://doi.org/10.1073/pnas.1812883116>.
- Rinaldi, M., Paglione, M., Decesari, S., Harrison, R.M., Beddows, D.C.S., Ovadnevaite, J., Ceburnis, D., O'Dowd, C.D., Simó, R., Dall'Osto, M., 2020. Contribution of Water-Soluble Organic Matter from Multiple Marine Geographic Eco-Regions to Aerosols around Antarctica. *Environmental Science & Technology* 54 (13), 7807–7817. <https://doi.org/10.1021/acs.est.0c00695>.
- Sarmiento, J.L., Gruber, N., 2006. *Ocean Biogeochemical Dynamics*. Princeton University Press.
- Scheuvs, D., Kandler, K., Küpper, M., Lieke, K., Zorn, R.S., Ebert, M., Weinbruch, S., 2011. Individual-particle analysis of airborne dust samples collected over Morocco in 2006 during SAMUM 1. *Tellus B* 63 (4), 512–530.
- Schroth, A.W., Crusius, J., Sholkovitz, E.R., Bostick, B.C., 2009. Iron solubility driven by speciation in dust sources to the ocean. *Nat. Geosci.* 2 (5), 337–340. <https://doi.org/10.1038/ngeo501>.
- Shoenfelt, E.M., et al., 2017. High particulate iron(II) content in glacially sourced dusts enhances productivity of a model diatom. *Sci. Adv.* 3 (6), e1700314. <https://doi.org/10.1126/sciadv.1700314>.
- Shoenfelt, E.M., Winckler, G., Lamy, F., Anderson, R.F., Bostick, B.C., 2018. Highly bioavailable dust-borne iron delivered to the Southern Ocean during glacial periods. *Proc. Natl. Acad. Sci.* 115 (44), 11180–11185. <https://doi.org/10.1073/pnas.1809755115>.
- Sholkovitz, E.R., Sedwick, P.N., Church, T.M., Baker, A.R., Powell, C.F., 2012. Fractional solubility of aerosol iron: synthesis of a global-scale data set. *Geochim. Cosmochim. Acta* 89, 173–189. <https://doi.org/10.1016/j.gca.2012.04.022>.
- Siefert, R.L., Pehkonen, S.O., Erel, Y., Hoffmann, M.R., 1994. Iron photochemistry of aqueous suspensions of ambient aerosol with added organic acids. *Geochim. Cosmochim. Acta* 58 (15), 3271–3279.
- Siebert, M., et al., 2019. The Antarctic peninsula under a 1.5°C global warming scenario. *Frontiers in environmental Science* 7 (102). <https://doi.org/10.3389/fenvs.2019.00102>.
- Spolaor, A., Vallenga, P., Cozzi, G., Gabrieli, J., Varin, C., Kehrwald, N., Zennaro, P., Boutron, C., Barbante, C., 2013. Iron speciation in aerosol dust influences iron bioavailability over glacial-interglacial timescales. *Geophys. Res. Lett.* 40 (8), 1618–1623. <https://doi.org/10.1002/grl.50296>.
- Tagliabue, A., Bowie, A.R., Boyd, P.W., Buck, K.N., Johnson, K.S., Saito, M.A., 2017. The integral role of iron in ocean biogeochemistry. *Nature* 543 (7643), 51.
- Takahashi, Y., Higashi, M., Furukawa, T., Mitsunobu, S., 2011. Change of iron species and iron solubility in asian dust during the long-range transport from western China to Japan. *Atmos. Chem. Phys.* 11 (21), 11237–11252.
- Vaughan, D.G., Marshall, G.J., Connolly, W.M., Parkinson, C., Mulvaney, R., Hodgson, D.A., King, J.C., Pudsey, C.J., Turner, J., 2003. Recent rapid regional climate warming on the Antarctic peninsula. *Clim. Chang.* 60 (3), 243–274. <https://doi.org/10.1023/A:1026021217991>.
- Vogt, S., 2003. MAPS: A set of software tools for analysis and visualization of 3D X-ray fluorescence data sets. Paper Presented at Journal de Physique IV (Proceedings), EDP Sciences.
- Weller, R., Wöltjen, J., Piel, C., Resenberg, R., Wagenbach, D., König-Langlo, G., Kriews, M., 2008. Seasonal variability of crustal and marine trace elements in the aerosol at Neumayer station, Antarctica. *Tellus B* 60 (5), 742–752. <https://doi.org/10.1111/j.1600-0889.2008.00372.x>.
- Wilke, M., Farges, F., Petit, P.-E., Brown Jr., G.E., Martin, F., 2001. Oxidation state and coordination of Fe in minerals: an Fe K-XANES spectroscopic study. *Am. Mineral.* 86 (5-6), 714–730. <https://doi.org/10.2138/am-2001-5-612>.
- Winton, V.H.L., Dunbar, G.B., Bertler, N.A.N., Millet, M.A., Delmonte, B., Atkins, C.B., Chewings, J.M., Andersson, P., 2014. The contribution of aeolian sand and dust to iron fertilization of phytoplankton blooms in southwestern Ross Sea, Antarctica. *Glob. Biogeochem. Cycl.* 28 (4), 423–436. <https://doi.org/10.1002/2013gb004574>.
- Xu, N., Gao, Y., 2008. Characterization of hematite dissolution affected by oxalate coating, kinetics and pH. *Appl. Geochem.* 23 (4), 783–793. <https://doi.org/10.1016/j.apgeochem.2007.12.026>.
- Xu, G., Gao, Y., 2014. Atmospheric trace elements in aerosols observed over the Southern Ocean and coastal East Antarctica. *Polar Res.* 33 (1), 23973. <https://doi.org/10.3402/polar.v33.23973>.
- Xu, G., Gao, Y., 2017. Characterization of atmospheric iron speciation and acid processing at metropolitan Newark on the US East Coast. *Atmosphere* 8 (4), 66.
- Zhu, X., Prospero, J.M., Millero, F.J., Savoie, D.L., Brass, G.W., 1992. The solubility of ferric iron in marine mineral aerosol solutions at ambient relative humidities. *Mar. Chem.* 38 (1), 91–107. [https://doi.org/10.1016/0304-4203\(92\)90069-M](https://doi.org/10.1016/0304-4203(92)90069-M).
- Zhu, X., Prospero, J.M., Savoie, D.L., Millero, F.J., Zika, R.G., Saltzman, E.S., 1993. Photoreduction of iron(III) in marine mineral aerosol solutions. *J. Geophys. Res. Atmos.* 98 (D5), 9039–9046. <https://doi.org/10.1029/93JD00202>.
- Znó, A., Chwedorzewska, K.J., Androsiuk, P., Cuba-Díaz, M., Gielwanowska, I., Koc, J., Korczak-Abshire, M., Grzesiak, J., Zmarz, A., 2017. Rapid environmental changes in the Western Antarctic peninsula region due to climate change and human activity. *Appl. Ecol. Environ. Res.* 15 (4), 525–539.